A Mindlin derived Dahl friction model

Nicolas Peyret, Marco Rosatello, Gael Chevallier, Jean-Luc Dion

▶ **To cite this version:**

Nicolas Peyret, Marco Rosatello, Gael Chevallier, Jean-Luc Dion. A Mindlin derived Dahl friction model. Mechanism and Machine Theory, 2017, 117, pp.48-55. 10.1016/j.mechmachtheory.2017.06.019 . hal-02131303

HAL Id: hal-02131303
https://hal.science/hal-02131303

Submitted on 3 Feb 2020

HAL is a multi-disciplinary open access archive for the deposit and dissemination of scientific research documents, whether they are published or not. The documents may come from teaching and research institutions in France or abroad, or from public or private research centers.

L'archive ouverte pluridisciplinaire **HAL**, est destinée au dépôt et à la diffusion de documents scientifiques de niveau recherche, publiés ou non, émanant des établissements d'enseignement et de recherche français ou étrangers, des laboratoires publics ou privés.

Distributed under a Creative Commons Attribution 4.0 International License

A Mindlin derived Dahl friction model

Nicolas Peyret [a,*], Marco Rosatello [a], Gaël Chevallier [b], Jean-Luc Dion [a]

[a] *Laboratoire Quartz, SUPMECA EA7393, Saint-Ouen, 93400 France*
[b] *FEMTO-ST Institute UMR6174, UBFC, ENSMM, UTBM, Besançon, 25000, France*

Friction modeling is essential in a vast amount of engineering applications. In this paper Mindlin contact friction model, a Masing rule compliant model, is manipulated in order to find a correlation with Dahl dynamic friction model, a Masing rule not compliant model. The resulting equations are then numerically compared and the correlation demonstrated with several loading functions. The result is a modified Dahl model that captures the partial slip behavior following the contact theory. The Dahl model, classically used in control engineering as an empirical model due to its implementation facility, finds in this new formulation a physical meaning to its parameters and finally identified physical parameters (according from Mindlin model) for the Dahl model.

1. Introduction

Friction plays a fundamental role in a wide variety of physical systems and the research community around this topic is always very active. The creation of models to accurately describe the phenomenon of friction has always been one of the main objectives of this research field, but the underlying reasons were different. For example, in the tribology field, friction models are needed in order to evaluate the fatigue life of bodies in contact, while for other disciplines, such as control engineering, friction models are necessary in order to develop control strategies that are able to compensate for the friction behavior.

Friction models can be divided into two main categories: macro-models and constitutive models.

Macro-models are based on empirical and experimental observations of the friction behavior and are divided in three main categories: quasi-static, dynamic and hysteretic models. Quasi-static models are the classical friction models, which assumes the friction force to be a function of the relative velocity of the contact surfaces. The simplest and also best-known quasi-static model is Coulomb's, from which other models were derived, in order to take into account phenomena such as viscous friction, Stribeck effect, stiction and kinetic friction.

Dynamic models are particularly used by control engineers and the first dynamic model was developed by Dahl [1], who derived it from the materials strain-rate equation. Further developments on Dahl's model brought to the creation of other models such as the Bliman–Sorine model [2], the Haessig and Friedland bristle model [3] and the one conceived by Canudas de Wit and al. in [4], best known as the LuGre model [5,6]. In automatic control domain, and especially in programmed handling activities, friction is an important physical phenomenon to master in order to ensure reliability and precision [7].

* Corresponding author.
E-mail addresses: nicolas.peyret@supmeca.fr (N. Peyret), marco.rosatello@supmeca.fr (M. Rosatello), gael.chevallier@univ-fcomte.fr (G. Chevallier), jean-luc.dion@supmeca.fr (J.-L. Dion).

Hysteretic models come from the theory of elasticity and they are used to model friction and energy dissipation in materials, geomechanics and jointed structures. Well-known hysteretic models are Masing model [8] and Iwan model [9], which are based on distributions of Jenkins elements.

Differently from macro-models, the constitutive models are derived from Hertz contact theory (see [10]), in order to describe the stress-strain relationship in the contact region. First Cattaneo [11] and then Mindlin [12], developed Hertz theory to take into account a tangential alternative load. This model is classically used in the study of fretting and wear in contact physics and in tribology domain.

The aim of this paper is, firstly, to find a correlation between the Mindlin model, which is a constitutive theoretical model that satisfies Masing rule [13], and Dahl's model, which instead is a dynamic empirical friction model that doesn't satisfy Masing rule, and secondly, the paper addresses to both Dahl and Mindlin model users: the goal is to provide physical parameters for Dahl model and an easier numerical implementation contact model.

In Section 2 the theory and the equations of the concerned friction models will be described . In Section 3, Mindlin's equations will be manipulated in order to find the correlation with Dahl's model and finally, in Section 4, a verification of the obtained correlation will be carried out. This correlation allows to give to the Dahl model, a new formulation with an analogy between the empirical model and the contact physics.

2. Theory

2.1. Mindlin contact model

In [11], Cattaneo studied the problem of the elastic contact between two bodies pressed on each other by a constant normal force N_0, with a tangential load T monotonically growing from zero to a maximum value T^*. Mindlin extended the model for a general oscillatory force of amplitude $\pm T^*$ and considered the contact between a sphere and a plane (see [10]).

From Hertz theory the radius a of the contact area is defined as:

$$a = \sqrt[3]{\frac{3}{4}\frac{N_0\rho}{E^*}} \tag{1}$$

where

$$\frac{1}{E^*} = \frac{1-\nu_1^2}{E_1} + \frac{1-\nu_2^2}{E_2} \tag{2}$$

and the generalized bending radius ρ is defined as:

$$\frac{1}{\rho} = \frac{1}{R_1} + \frac{1}{R_2} \tag{3}$$

being E_1, E_2 the Young moduli; ν_1^2, ν_2^2 the squares of the Poisson ratios and R_1, R_2 the bending radii of the two surfaces in contact.

In order to describe the friction behavior at the contact surface, both Cattaneo and Mindlin used the Coulomb's law. Considering μ the friction coefficient, if the tangential load T reaches the critical value

$$T_c = \mu N_0 \tag{4}$$

the two surfaces starts to slide relatively to each other entering in what is usually called the sliding or macro-slip phase, during which the tangential load T will remain constant.

During the monotonic tangential loading phase, Mindlin and Cattaneo demonstrated that the contact area is divided into two parts: a stick zone and a slip zone. The stick zone is a circle of radius c, while the slip zone is the annulus of internal radius c and external radius a. In Fig. 1b is possible to see the two regions, while in Fig. 1a are shown the normal and tangential stress distribution at the contact interface. The relationship between the stick zone radius c and the contact radius a was found by Cattaneo to be:

$$\frac{c}{a} = \left(1 - \frac{T}{\mu N_0}\right)^{\frac{1}{3}} \tag{5}$$

It's easy to see that, when the tangential load T increases, the stick region becomes smaller, until $T = T_c$, when $c = 0$ and the macro-slip phase takes place. Therefore, when $0 < T < T_c$, the contact is in a phase called partial slip. If we consider A_c as the contact area of radius a and A_s as the slip annular area of internal radius c and external radius a, some researchers prefer to divide this phase into a micro-slip phase, where $A_s << A_c$ and a partial slip phase, where $A_s < A_c$.

We now consider an oscillating loading cycle of amplitude $\pm T^*$. The hysteresis cycle has the shape of the one shown in Fig. 2, with the tangential displacement δ on the x-axis and the tangential force T on the y-axis. The cycle can be divided in three phases: initial loading from point O to point A (phase 0), unloading and reloading from point A to point C (phase 1), unloading and reloading back from point C to point A (phase 2).

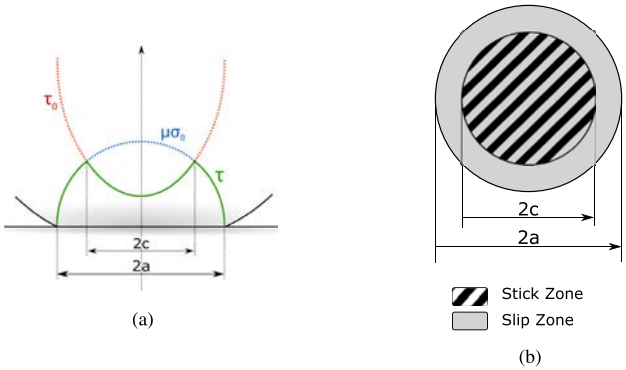

Fig. 1. Stress distribution at the contact interface (a) and contact area (b) for a contact between a sphere and a plane with a tangential force $T < T_c$.

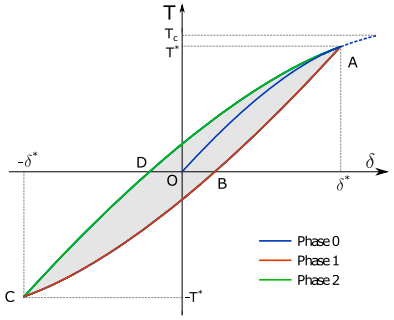

Fig. 2. General hysteresis cycle and its phases.

According to Mindlin model in [10], it's possible to write the tangential displacement δ as a function of the applied tangential force T. During the initial loading the tangential displacement δ_0 can be written as:

$$\delta_0 = \frac{3\mu N_0 G^*}{16a}\left(1 - \left(1 - \frac{T}{\mu N_0}\right)^{\frac{2}{3}}\right) \tag{6}$$

where

$$G^* = \frac{2-\nu_1}{G_1} + \frac{2-\nu_2}{G_2} \tag{7}$$

in which G_1 and G_2 are the shear moduli of the materials in contact. During the unloading and reloading phases, the respective tangential displacements δ_1 and δ_2 can be written as:

$$\delta_1 = \frac{3\mu N_0 G^*}{16a}\left[2\left(1 - \frac{T^* - T}{2\mu N_0}\right)^{\frac{2}{3}} - \left(1 - \frac{T^*}{\mu N_0}\right)^{\frac{2}{3}} - 1\right] \quad \text{Phase 1} \tag{8}$$

$$\delta_2 = -\frac{3\mu N_0 G^*}{16a}\left[2\left(1 - \frac{T^* + T}{2\mu N_0}\right)^{\frac{2}{3}} - \left(1 - \frac{T^*}{\mu N_0}\right)^{\frac{2}{3}} - 1\right] \quad \text{Phase 2} \tag{9}$$

It's important to point out that, if the tangential force T reaches the critical value $T_c = \mu N_0$, according to Coulomb's friction model, it will remain constant until the load changes direction.

2.2. Dahl friction model

Dahl friction model [1] was introduced in 1968 to study the rolling friction in ball bearings. Dahl's main idea was to use the materials stress-strain curve of classical solid mechanics in order to model friction. Considering T to be the friction force and $T_c = \mu N$ its critical value according to Coulomb's law, Dahl's model general form is:

$$\frac{dT}{dx} = \sigma\left[1 - \frac{T}{T_c}sign(\dot{x})\right]^{\alpha} \tag{10}$$

where σ is the stiffness coefficient, which represents the slope of the curve at $T = 0$, while α is a parameter that determines the shape of the curve and it's usually taken as $\alpha = 1$. Furthermore, the force $|T|$ will never be larger than the critical value T_c.

It's possible to see that in this model the friction force is only function of the displacement x and of the sign of the velocity $\dot{x}$.

2.3. Masing models

Masing models are simple tools for describing the hysteretic behavior of many systems. The model was firstly introduced to model the Bauschinger effect in materials (see [14]), which is a reduction in compression strength after a plastic deformation in tension.

Masing [13] was the first to create a model for elasto-plastic material during cycle loading. His theory provides also for the so called Masing rule or hypothesis, which says that the hysteresis paths during cycle loading can be obtained from the monotonic initial loading, also called "backbone" curve, with an expansion factor of two.

By keeping the notation shown in Fig. 2 the mathematical representation of Masing rule is the following:

$$\delta_1(T) = \delta^* - 2\delta_0\left(\frac{T^* - T}{2}\right) \tag{11}$$

where δ^* represents the maximum tangential displacement amplitude reached in the last cycle. A practical consequence of this rule, which is also a material property during cycle loading, is that the slope right after the load inversion has the same value of the initial slope during the monotonic initial loading phase. It's important to clarify that the original Masing hypothesis is only valid for steady-state cycles or loading between fixed limits.

At this point it's possible to check if the previously described Mindlin and Dahl models satisfy Masing rule. By applying Eqs. (11)–(13) it's possible to obtain Eq. (14), proving that Mindlin contact model is a Masing model.

If now we consider Dahl model, since Eq. (10) represents the instantaneous slope of the hysteresis curve in the plane $x - F$, it's easy to verify that:

$$\frac{dT}{dx}(0, \dot{x} > 0) = \sigma \neq \frac{dT}{dx}(T^*, \dot{x} < 0) = \sigma\left(1 + \frac{T^*}{T_c}\right)^{\alpha} \tag{12}$$

which means that Dahl model does not satisfy Masing hypothesis.

The Masing assumption allows to deduce the full hysteresis cycle only by knowing the first quarter of it, instead of having to compute the complete and closed cycle. For example, this is particularly useful when the dissipated energy per cycle has to be calculated. If the model satisfies Masing hypothesis, you can just compute the dissipated energy during the initial loading and multiply this value by four to obtain the dissipated energy in the closed hysteresis cycle.

2.4. Correlation between Mindlin and Dahl models

After having described the two models in the previous sections, a correlation procedure is now shown.

The first step is to find the expression of the tangential force T as a function of the displacement δ from Eqs. (6) to (9). The equations of the tangential force T during the different phases of the hysteresis cycle can then be written as:

$$T_0 = \mu N_0\left[1 - \left(1 - \frac{16a}{3\mu N_0 G^*}\delta_0\right)^{\frac{3}{2}}\right] \tag{13}$$

$$T_1 = T^* - 2\mu N_0\left[1 - \left[\frac{1}{2}\left(\frac{16a}{3\mu N_0 G^*}\delta + \left(1 - \frac{T^*}{\mu N_0}\right)^{\frac{2}{3}} + 1\right)\right]^{\frac{3}{2}}\right] \tag{14}$$

$$T_2 = -T^* + 2\mu N_0\left[1 - \left[\frac{1}{2}\left(\frac{16a}{3\mu N_0 G^*}\delta + \left(1 - \frac{T^*}{\mu N_0}\right)^{\frac{2}{3}} + 1\right)\right]^{\frac{3}{2}}\right] \tag{15}$$

At this point the derivatives of Eqs. (13)–(15) with respect to the variable δ are found as:

$$\frac{dT_0}{d\delta_0} = \frac{8a}{G^*}\left(1 - \frac{16a}{3\mu N_0 G^*}\delta\right)^{\frac{1}{2}} \tag{16}$$

$$\frac{dT_1}{d\delta} = \frac{8a}{\sqrt{2}G^*}\left[1 + \frac{16a}{3\mu N_0 G^*}\delta + \left(1 - \frac{T^*}{\mu N_0}\right)^{\frac{2}{3}}\right]^{\frac{1}{2}} \tag{17}$$

$$\frac{dT_2}{d\delta} = \frac{8a}{\sqrt{2}G^*}\left[1 - \frac{16a}{3\mu N_0 G^*}\delta + \left(1 - \frac{T^*}{\mu N_0}\right)^{\frac{2}{3}}\right]^{\frac{1}{2}} \tag{18}$$

Finally Eqs. (6)–(9) are replaced respectively in Eqs. (16)–(18), obtaining:

$$\frac{dT}{d\delta_0} = \frac{8a}{G^*}\left(1 - \frac{T}{T_c}\right)^{\frac{1}{3}} \qquad \text{Phase 0} \tag{19}$$

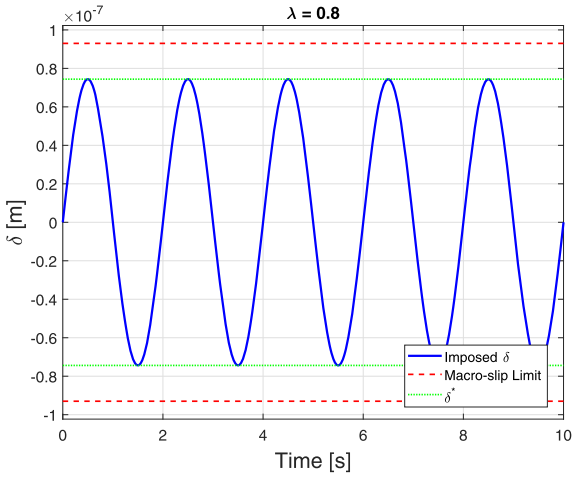

(a) Micro-slip excitation ($\lambda = 0.8$)

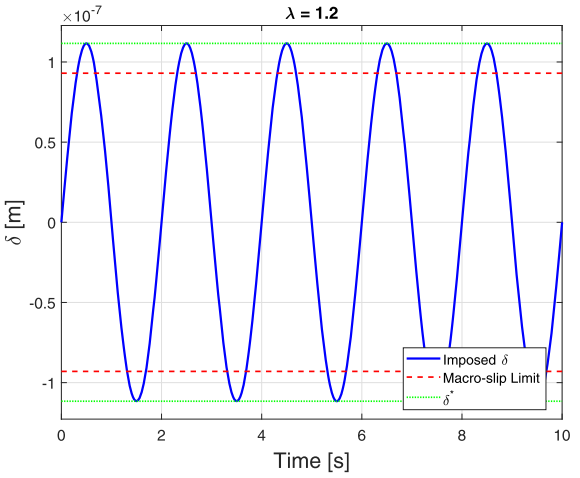

(b) Macro-slip excitation ($\lambda = 1.2$)

Fig. 3. Imposed displacement excitation.

$$\frac{dT}{d\delta} = \frac{8a}{G^*}\left(1 - \frac{T^* + T\,sign(\dot{\delta})}{2T_c}\right)^{\frac{1}{3}} \qquad \text{Phase 1\&Phase 2} \tag{20}$$

If we analyze these last two equations, it's possible to see that they are equivalent to the original Dahl friction model of Eq. (10) with the two parameters σ and α chosen as(See Peyret in [15]:

$$\sigma = \frac{8a}{G^*} \qquad \alpha = \frac{1}{3} \tag{21}$$

Therefore, Eqs. (19)–(20) represent the Mindlin–Dahl correlated model.

3. Results and discussion

In order to validate the model and compare the model, a tangential displacement

$$\delta = \lambda\delta_c \sin(2\pi t) \tag{22}$$

is imposed to the model, in which δ_c is the critical displacement at which the friction force becomes equal to the Coulomb friction and macro-slip occurs:

$$\delta_c = \frac{3\mu N G^*}{12a} \tag{23}$$

where λ is an dimensionless coefficient. If $\lambda \geq 1$, macro-slip occurs. The values of the parameters set used in simulations are, for Dahl's model: $\sigma = 4.839e+08$, $\alpha = 1/3$; for Mindlin's model : $\mu = 0.3$, $N = 100$ [N], $a = 0.0027$ [m], $G^* = 4.42e-11$ [1/Pa]

Fig. 3 shows the two excitation functions applied to the models: in Fig. 3a the imposed displacement remains inside the micro-slip regime, while in Fig. 3b macro-slip occurs.

Concerning the numerical resolution of the models, for Mindlin's model there are no particular problems, while for the correlated Dahl model, the derivation in respect of time must be found. The latter is obtained as:

$$\frac{dT}{dt} = \frac{dT}{d\delta}\frac{d\delta}{dt} = \sigma\dot{\delta}\left(1 - \frac{T}{T_c}\right)^{\alpha} \tag{24}$$

where

$$\dot{\delta} = 2\pi\lambda\delta_c \cos(2\pi t) \tag{25}$$

At this point the displacement functions shown in Fig. 3, one for micro-slip with $\lambda = 0.8$ and one for macro-slip with $\lambda = 1.2$, are applied to three different models. The first model is, of course, Mindlin's model, represented by Eqs. (13)–(15). The second is Dahl's correlated model integrated in time and represented by the following equations:

$$\dot{T} = \sigma\dot{\delta}\left(1 - \frac{T}{T_c}\right)^{\alpha} \qquad \text{Phase 0} \tag{26}$$

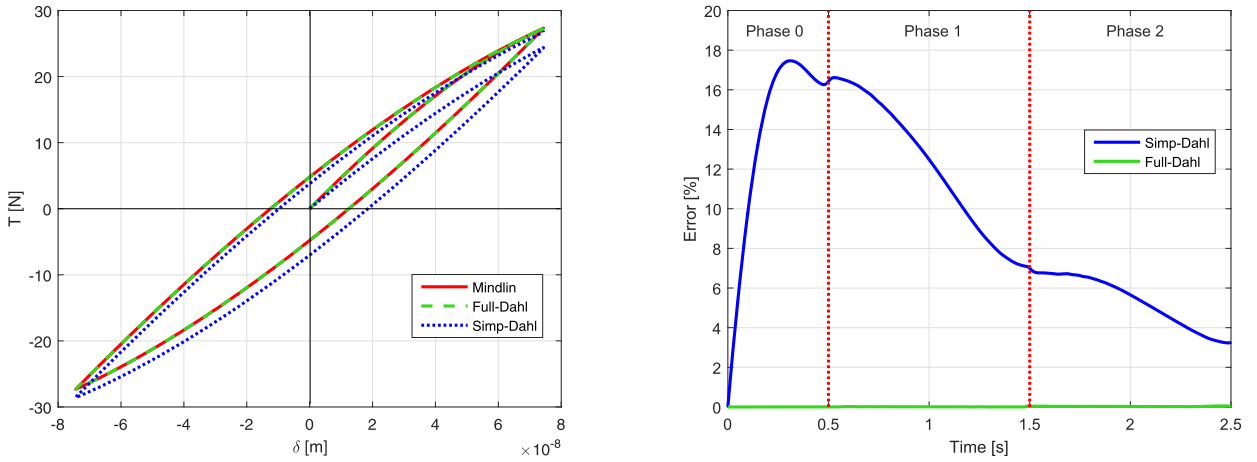

Fig. 4. Comparison between Mindlin, Full-Dahl and Simplified-Dahl during a full cycle of micro-slip excitation.

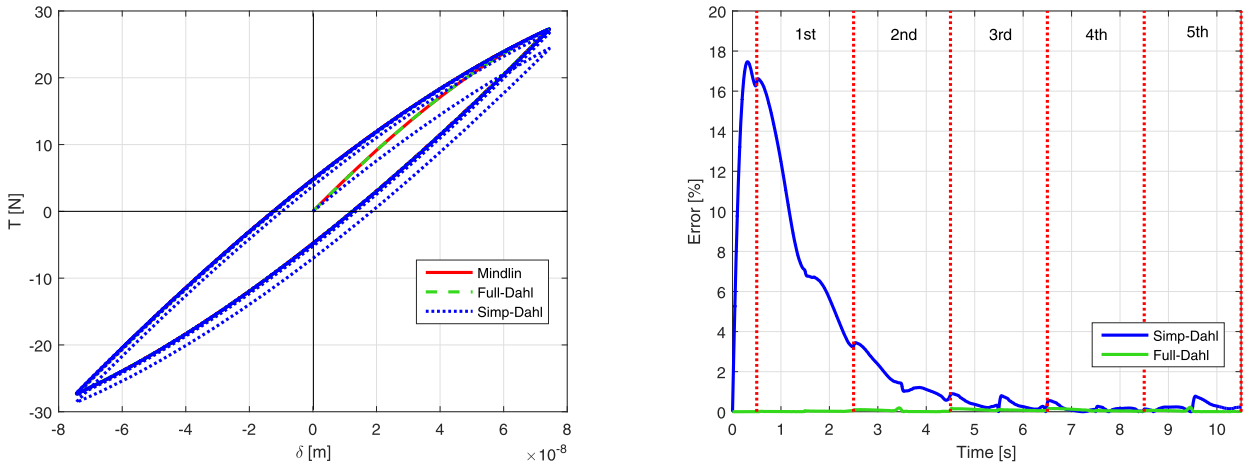

Fig. 5. Comparison between Mindlin, Full-Dahl and Simplified-Dahl during 5 cycles of micro-slip excitation.

$$\dot{T} = \sigma\dot{\delta}\left(1 - \frac{T^* + Tsign(\dot{\delta})}{2T_c}\right)^{\alpha} \qquad \text{Phase 1\&Phase 2} \tag{27}$$

This model will be referred as *Full-Dahl*. Ultimately, the third model is again Dahl's correlated model, but this time ignoring Eq. (26) for the initial loading, thus using only Eq. (27). In order to distinguish it from the *Full-Dahl*, this model will be referred as *Simplified-Dahl*.

In the model comparison process, firstly only one full hysteresis cycle as represented in Fig. 2 is considered: Fig. 4a shows the tangential friction force as a function of the displacement for the three models previously described, while Fig. 4b shows the percentage error of the correlated Dahl's models relative to the original Mindlin model. Full-Dahl model correctly follows Mindlin's model, with a percentage error always smaller than 2%. Concerning the Simplified-Dahl model, after the initial loading phase which obviously produces a consistent error, the latter decreases throughout the unloading and reloading phases, but it remains unacceptable.

However, if we consider the experiments in the tribology and material fatigue domain, the number of cycles considered is high. Fig. 5 shows the behavior of the models for a higher number of cycles: it's possible to notice that, after about 3 cycles, the percentage error of the Simplified-Dahl model reaches the level of the Full-Dahl one, thus it becomes acceptable, being always under 2%.

The results discussed until now are referred to the imposed displacement function shown in Fig. 3a, which implies an hysteresis cycle entirely inside the micro-slip domain. In order to obtain the behavior during the macro-slip phase, the

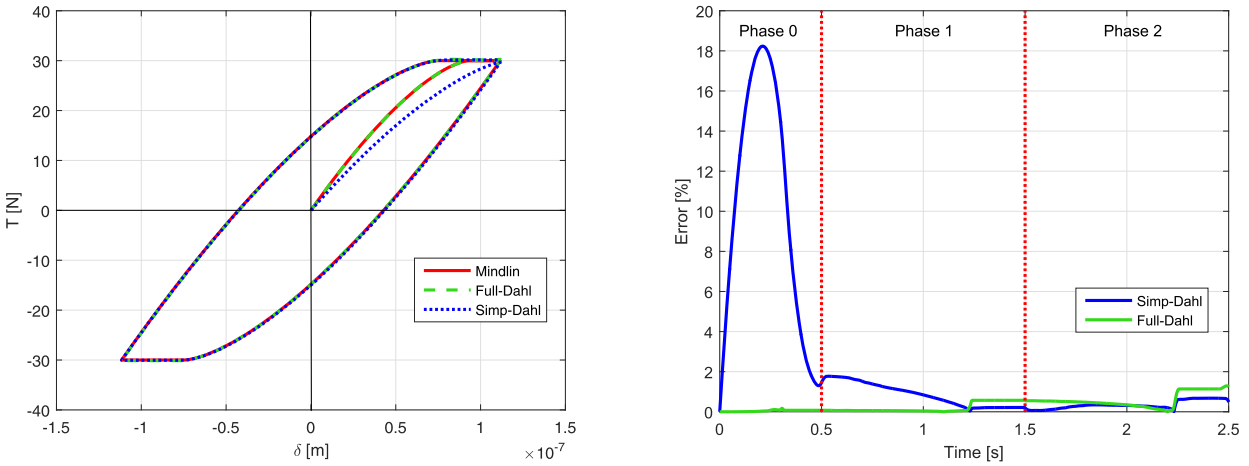

Fig. 6. Comparison between Mindlin, Full-Dahl and Simplified-Dahl for one cycle in a macro-slip situation.

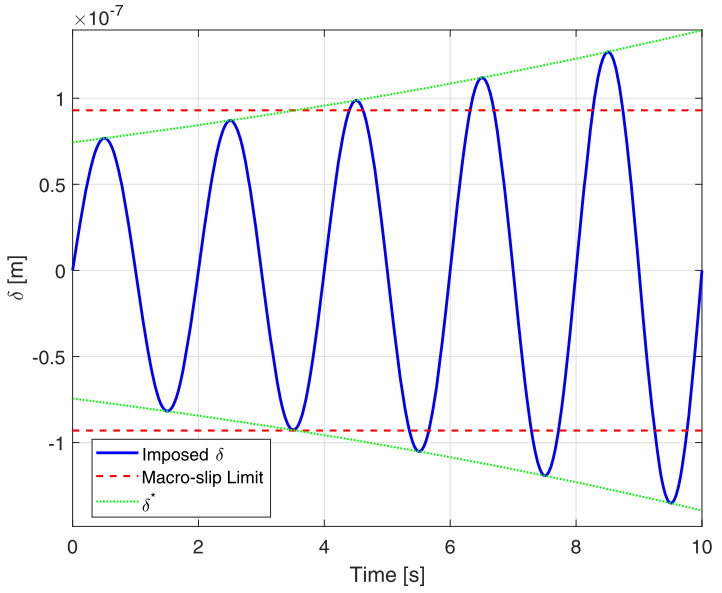

Fig. 7. Exponential growing sinus excitation.

imposed displacement function of Fig. 3b is applied, and the results are shown in Fig. 6, where the tangential effort and the percentage error are calculated over one full cycle. It's possible to see that, for the loading phase, the behavior of the different models is the same, with a consistent error for the Simplified-Dahl model. After this phase, however, the behavior changes, assisting to a fast decrease in the Simplified-Dahl error, which becomes even lower than the Full-Dahl one: this aspect can be simply due to numerical errors. Thus, in this case, the error of the simplified model becomes acceptable right after the loading phase, and not after a few cycles as it was shown for the micro-slip case of Fig. 5a.

After having obtained good results with a simple sinus excitation, which is also one of the condition imposed by Mindlin, the exponential growing sinus represented in Fig. 7, is applied to the models. It's possible to see that at the beginning the function is within the micro-slip and after some cycles enters in the macro-slip phase. Since the amplitude δ^* of the excitation is not constant, it was calculated at each step as the envelope of the loading function, represented by the green dot lines in Fig. 7. The results of the application of this particular excitation produces the results shown in Fig. 8: it's possible to say that there is a good matching even if the assumptions of Mindlin model are not respected(steady sine excitation of amplitude T^*). The percentage error shows the behavior already seen for the simple sinus excitation, but in this case there is a residual varying error that probably depends on the way the maximum amplitude δ^* is calculated.

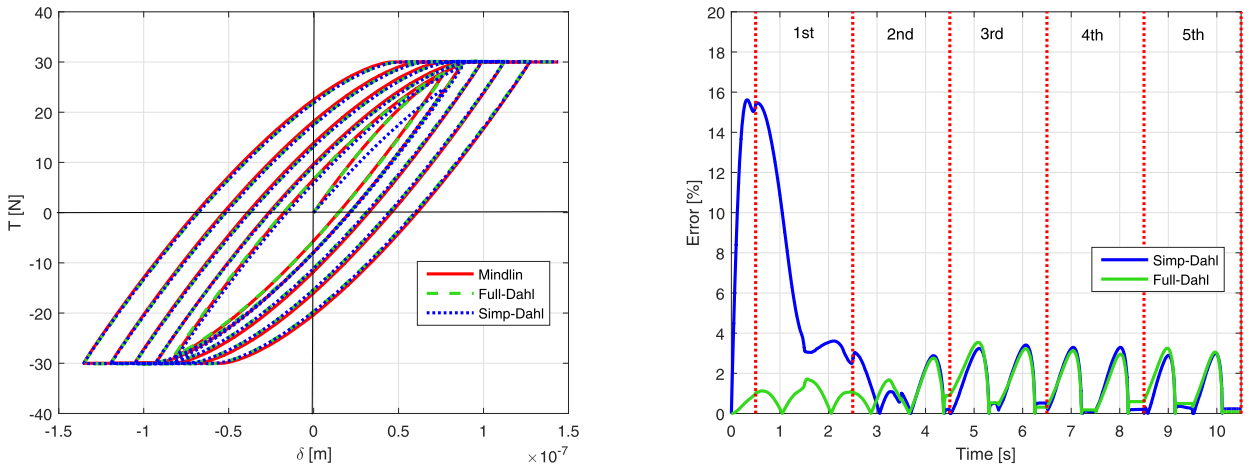

(a) (b)

Fig. 8. Comparison between Mindlin, Full-Dahl and Simplified-Dahl during 5 cycles of exponential excitation.

4. Conclusions

In the paper, two well-known friction models, belonging to two different categories of models, were presented. It was demonstrated that, by mathematically manipulating the Mindlin's model equations, it's possible to find an alternative formulation of the Dahl dynamic friction model. The models were then validated through the application of different excitation functions and the error in respect to Mindlin's model was evaluated.

The interesting aspects of the obtained results are several: firstly, considered that Mindlin's model observes the Masing rule, while this is not satisfied by Dahl's model, the correlation was able to find a Masing rule compliant Dahl model. Secondly, Mindlin's model is composed by three different equations, each one for a different phase of the hysteresis cycle: The Full-Dahl model is also composed by three differential equations, but it was shown to be precise enough with only two (Simplified Dahl). The latter aspect implies an easier numerical implementation and it can be used as a friction model, not only in tribology, but also in other contexts, when it's necessary to accurately represent accurately the micro-slip phase, and probably most importantly, this work allowed to connect Dahl model, which began as an empirical global behavior law, to the contact physics.

Finally, on one hand, Dahl model is an easy-to-use model with only 3 empirical parameters, without any physical meaning. On the other hand, Mindlin model is realistic and based on clear physical parameters, but these are numerous, making it still difficult to use with reasonable computation costs. Our work allows to exploit the advantages of both models, while avoiding their drawbacks. The bottom line is that we have linked the Dahl parameters to the Mindlin physical ones, which allows us to use the easy-to-compute Dahl model with parameters that are linked to the actual physics of parts and surfaces in contact.

References

[1] P. Dahl, A Solid Friction Model, Technical Report, DTIC Document, 1968.
[2] P. Bliman, M. Sorine, Friction modeling by hysteresis operators. application to dahl, sticktion and stribeck effects, Pitman Research Notes in Mathematics Series(1993) 10.
[3] D.A. Haessig, B. Friedland, On the modeling and simulation of friction, J. Dyn. Syst. Meas. Contr. 113 (3) (1991) 354–362.
[4] C.C. De Wit, H. Olsson, K.J. Astrom, P. Lischinsky, A new model for control of systems with friction, Autom. Contr., IEEE Trans. 40 (3) (1995) 419–425.
[5] J. Dion, G. Chevallier, O. Penas, F. Renaud, A new multicontact tribometer for deterministic dynamic friction identification, Wear 300 (1) (2013) 126–135.
[6] T. Piatkowski, Dahl and lugre dynamic friction models – the analysis of selected properties, Mech. Mach. Theory 73 (2014) 91–100.
[7] T. Piatkowski, Analysis of translational positionning of unit loads by directionally-oriented friction force fields, Mech. Mach. Theory 46 (2011) 201–217.
[8] G. Masing, Zur heynschen theorie der verfestigung der metalle durch verborgen elastische spannungen, in: Wissenschaftliche Veröffentlichungen aus dem Siemens-Konzern, Springer, 1923, pp. 231–239.
[9] W.D. Iwan, A distributed-element model for hysteresis and its steady-state dynamic response, J. Appl. Mech. 33 (4) (1966) 893–900.
[10] K. Johnson, Contact Mechanics, Cambridge university press, 1987.
[11] C. Cattaneo, Sul contatto di due corpi elastici: distribuzione locale degli sforzi, Rend. Accad. Naz. Lincei 27 (6) (1938) 342–348.
[12] R. Mindlin, Compliance of elastic bodies in contact, J. Appl. Mech. 16 (2013).
[13] G. Masing, Eigenspannungen und verfestigung beim messing, in: Proceedings of the 2nd International Congress of Applied Mechanics, 100, sn, 1926, pp. 332–335.
[14] R. Skelton, H. Maier, H.-J. Christ, The bauschinger effect, masing model and the ramberg–osgood relation for cyclic deformation in metals, Mater. Sci. Eng. 238 (2) (1997) 377–390.
[15] N. Peyret, Dissipation de l'énergie mécanique dans les assemblages: effet du frottement en sollicitation dynamique, Université Paris-Est, 2012 Ph.D. thesis.